Jinlong Liu

Department of Mechanical and Aerospace
Engineering,
Center for Alternative Fuels Engines and
Emissions (CAFEE),
West Virginia University,
Morgantown, WV 26506-6106
e-mail: jlliu@mix.wvu.edu

Hemanth Kumar Bommisetty

Department of Mechanical and Aerospace
Engineering,
Center for Alternative Fuels Engines and
Emissions (CAFEE),
West Virginia University,
Morgantown, WV 26506-6106
e-mail: hebommisetty@mix.wvu.edu

Cosmin Emil Dumitrescu[1]

Department of Mechanical and Aerospace
Engineering,
Center for Alternative Fuels Engines and
Emissions (CAFEE) and Center for Innovation in
Gas Research and Utilization (CIGRU),
West Virginia University,
Morgantown, WV 26506-6106
e-mail: cedumitrescu@mail.wvu.edu

Experimental Investigation of a Heavy-Duty Compression-Ignition Engine Retrofitted to Natural Gas Spark-Ignition Operation

Heavy-duty compression-ignition (CI) engines converted to natural gas (NG) operation can reduce the dependence on petroleum-based fuels and curtail greenhouse gas emissions. Such an engine was converted to premixed NG spark-ignition (SI) operation through the addition of a gas injector in the intake manifold and of a spark plug in place of the diesel injector. Engine performance and combustion characteristics were investigated at several lean-burn operating conditions that changed fuel composition, spark timing, equivalence ratio, and engine speed. While the engine operation was stable, the reentrant bowl-in-piston (a characteristic of a CI engine) influenced the combustion event such as producing a significant late combustion, particularly for advanced spark timing. This was due to an important fraction of the fuel burning late in the squish region, which affected the end of combustion, the combustion duration, and the cycle-to-cycle variation. However, the lower cycle-to-cycle variation, stable combustion event, and the lack of knocking suggest a successful conversion of conventional diesel engines to NG SI operation using the approach described here. [DOI: 10.1115/1.4043749]

Introduction

Natural gas (NG) is a low-carbon fuel that has the potential to lower the demand of petroleum-based fuels, reduce engine-out emissions, and increase the thermal efficiency (η_{th}) of internal combustion (IC) engines [1–4]. Also, NG can decrease carbon dioxide (CO_2) emissions at similar power output because of its higher hydrogen-to-carbon ratio compared with gasoline and diesel [3,5]. Compared with diesel, NG mixes better with air, which avoids the creation of fuel-rich regions inside the cylinder and thus reduces particulate matter (PM) emissions [5,6]. The wider flammability of NG compared with gasoline allows an engine to run leaner, which can reduce the carbon monoxide (CO), unburned hydrocarbon (HC), and nitrogen oxide (NO_x) emissions and increase efficiency [5–8]. NG's higher resistance to autoignition allows the engine to operate at a higher compression ratio (CR), increasing η_{th} [3,9]. In addition, the combination of a higher CR and a lean mixture results in a more effective utilization of the available energy and decreases the use of residual exhaust gases, which will increase flame speed while limiting in-cylinder temperature [10]. Consequently, lean-burn and high compression ratio heavy-duty NG engines are capable of close-to-diesel efficiency but with lower emissions levels compared with a conventional stoichiometric SI engine [3,11].

NG's higher resistance to autoignition compared with gasoline benefits thermal efficiency in spark-ignition (SI) applications but increases the difficulty in initiating and controlling the combustion process in compression-ignition (CI) applications without the use of an additional ignition source [12,13]. Pilot-ignition using a more-reactive fuel and spark-ignition are two solutions to ignite the NG/air mixture in CI engines converted to NG [14]. Pilot-ignition (e.g., using diesel fuel) increases engine cost and

control complexities as it requires two fuel tanks, two separate fuel supply systems, and other engine and control modifications [15,16]. On the other hand, high-energy NG spark plugs ensure reliable ignition and repeatable combustion events [17]. For a cost-oriented market like the United States, manufacturers prefer the more economical solution, which is to convert existing gasoline or diesel engines to NG SI operation with the least amount of engine and control modifications [5,13].

NG's lower flammability limit makes it attractive for lean-burn applications, but its lower laminar flame speed compared with other hydrocarbons may be a challenge [3]. It was reported that the roof-type head geometry in conventional SI engines is not optimal for lean combustion due to combustion instabilities and increased cycle-to-cycle variations [3]. The resulting poor quality of combustion in such geometries under lean conditions decreases engine efficiency and increases HC and CO emissions [18]. As a result, gasoline engines with a roof-type head are more likely to be modified to NG stoichiometric operation. However, a fast-burn combustion chamber such as bowl-in-piston or nebula chambers would favor NG lean combustion [3]. Fast-burn combustion chambers generate high turbulence (swirl, tumble, squish, etc.) near top dead center (TDC) [19], which would enhance the flame speed in lean-burn applications. Consequently, one efficient use of NG in the transportation sector would be as a direct replacement of the diesel fuel in CI engines without any major engine modifications to the combustion chamber such as new pistons and/or engine head [20,21]. As the conventional geometry of a CI engine (i.e., reentrant bowl and flat head) is a fast-burn chamber, adding a spark plug in the place of the diesel injector can initiate and control the NG combustion process under lean conditions [22,23]. Specifically, a bowl-in-piston geometry creates a sudden and abrupt turbulence (radial flow) as the piston approaches TDC. Moreover, a tumble flow is generated by the squish and upward-moving piston close to TDC. The combination of tumble and intake swirl was shown to be effective in enhancing and stabilizing the combustion, therefore increasing the burn rates [19]. Moreover, while this very intensive motion is located at the region between the reentrant wall and bowl crown, the region around the spark plug

---

location experiences a more moderate turbulence, which helps with the ignition process.

A review of the (limited) literature on CI converted to SI NG operation indicated that the main focus was on evaluating the efficiency of existing aftertreatment systems on the emissions of vehicles equipped with such retrofitted CI engines [24,25]. As a result, the limited knowledge of the characteristics of NG combustion in diesel-like engines [26] can delay the conversion/introduction of heavy-duty NG vehicles. Moreover, some studies investigated the combustion characteristic for fuels with different properties compared with NG such as propane and butane [27–30] because that was the fuel of interest at that period. The limited experimental data is also reflected in the reduced number of 3D CFD investigations of CI engines converted to SI NG operation [13,14,31–33]. Based on all the above, the main goal of this study was to provide additional information on the NG combustion characteristics and performance inside a diesel-like combustion chamber under different operating conditions that changed spark timing, mixture equivalence ratio, and engine speed beyond the preliminary studies in Ref. [8]. The effect of fuel composition is another major concern for lean-burn high-CR NG engines, in addition to the lower flame speed, difficulties in igniting the fuel, and knock tendencies [3]. Consequently, the information on real fuel effects, spark and combustion stability, and cycle-to-cycle variations provided here can support the successful conversion of conventional diesel engines to NG SI operation.

Experimental Setup

Experiments were conducted in a single-cylinder, four-stroke, port fuel injection, heavy-duty spark ignited engine (Ricardo/Cussons, UK, Model Proteus) at West Virginia University (WVU) Advanced Combustion Laboratory. Figure 1 shows the experimental setup and Table 1 shows the engine specifications. The original supercharged, direct injection engine configuration (Volvo, Model TD 120) was modified to a spark ignited engine through replacing the main injector with an NG spark plug (Stitt, Conroe, TX, Model S-RSGN40XLBEX8.4-2), as shown in Fig. 1(c). NG was delivered inside the intake manifold using a gas injector (Rail Spa, Italy, Model IG7 Navajo, 3 seats), shown in Figs. 1(c) and 1(d). The mixture of the NG and air was formed in the inlet manifold, so the level of premixing was high and almost constant. The combustion chamber included a toroidal bowl-in-piston with swirl-producing intake ports, shown in Fig. 1(d). Swirl caused a counterclockwise rotational motion of the air-fuel mixture in the cylinder. Despite the off-center position of the piston bowl relative to the combustion chamber axis in this two-valve engine, the spark plug was located on the combustion bowl centerline. For the intake system, filtered intake air passed through a laminar flow element (LFE; Meriam, Cleveland, OH, Model Z50MC2-2), where a thermocouple was mounted at upstream to correct for variations in air density. A 30-gallon intake air surge tank, together with pressure snubbers, shown in Fig. 1(b), was installed after LFE to dampen the pressure pulsations caused by single-cylinder cyclic intake valve opening and closing, which was proved effective in dampening the intake air pressure fluctuations up to 83% from previous studies. Engine cooling was achieved by a personal-built closed system consisting of a pressurized header tank, pump (Boss, Model BK2507/10B), flow meter, heater (6 kW), filter, and heat exchangers. The lubrication system consisted of an oil sump/reservoir, heater, pump (Brook Crompton Parkinson Motors), filter, and heat exchangers. The oil pressure was relieved to 4 bars and supplied to the main bearings, big end bearing, camshaft bearings, and cylinder head. In addition, a 75-kW trunnion-type DC electrical dynamometer (McClure, Model 4999, Trunnion type), rated at 420 V and 160 A, operated through a thyristor bank (KTK, Model 6P4Q75), shown in Fig. 1(a), controlled the engine speed regardless of the engine load. A 100-kg load cell (Tedea-Huntleigh,
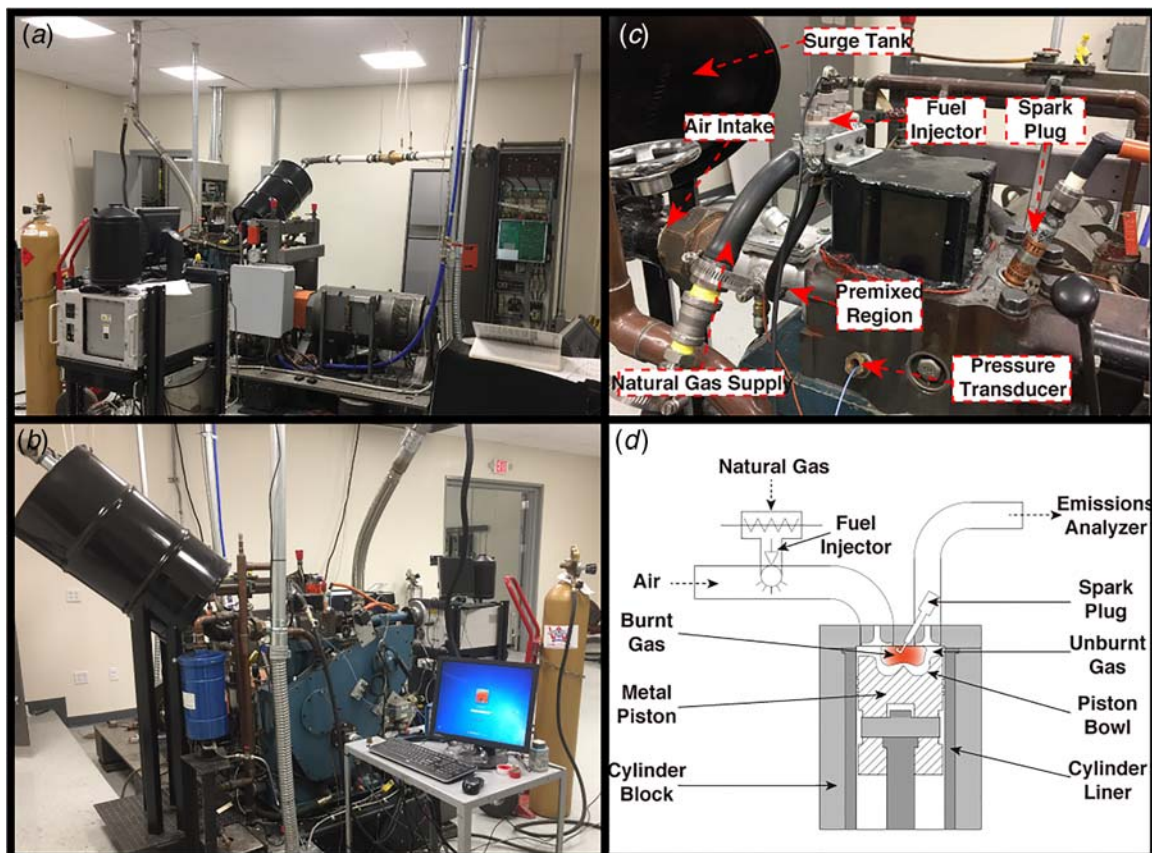

Fig. 1 Experimental setup: (a), (b) engine test cell, (c) top engine view, and (d) engine schematic

Table 1 Engine specifications

Manufacturer and model	Ricardo/Cussons, Proteus
Research engine type	Single-cylinder
Cycle	4-stroke SI premixed
Valves per cylinder	2
Bore (mm) × stroke (mm)	130.2 × 150
Displacement (liters)	1.997
Intake valve opens/close	12 CAD BTDC/140 CAD BTDC
Exhaust valve opens/closes	126 CAD ATDC/10 CAD ATDC
Connecting rod length (mm)	275
Connecting rod offset	None
Squish height (mm)	2
Compression ratio	13.3:1
Combustion chamber	Reentrant bowl and flat head

Table 2 Composition and selected properties of test gases

Components	Methane	Natural gas
CH_4 (vol%)	99.5%	Balance
C_2H_6 (vol%)	<1000 ppm	5.81%
C_3H_8 (vol%)	—	2.39%
$n\text{-}C_4H_{10}$ (vol%)	—	0.45%
$iso\text{-}C_4H_{10}$ (vol%)	—	0.421%
N_2 (vol%)	<4000 ppm	0.02%
O_2 (vol%)	<50 ppm	—
H_2O (vol%)	<10 ppm	—
H/C ratio	4.0	3.77
LHV (MJ/m^3)	35.88	41.79
Density (kg/m^3)	0.6682	0.7471
MON (-)	140.1	123.1
Methane number (-)	108.4	80.8
Wobbe index (MJ/Nm^3)	48.2	53.1

Table 3 Engine operating conditions

Spark timing[a] (CAD ATDC)	−30, −25, −20, −15, **−10**[b]
Equivalence ratio[c] (-)	CH_4: 0.71, **0.73**, 0.76, 0.8
	NG: 0.69, **0.71**, 0.74, 0.76
Engine speed (rpm)	**900**, 1000, 1100, 1200, 1300

[a]A controller malfunction during the spark time sweep was discovered during data analysis. As a result, the spark time sweep was repeated, but only for methane (i.e., there is no spark time sweep data for NG).
[b]This test condition used in the spark timing sweeping has identical operating conditions with the baseline. The repeated test showed almost the same results compared with baseline conditions. During the analysis in the next sections, the repeated tests were used in effects of changed spark timing and the original tests with baseline conditions were applied in other conditions effects.
[c]Higher molecular weight of NG and increased viscosity of higher alkanes present in NG would reduce the flow of NG through injectors. The mass of fuel injected is also proportional to the fuel density. They together resulted in different equivalence ratios of CH_4 and NG under similar injection duration.

Basingstoke Hants, UK, Model 104H) measured the torque applied on the dynamometer using a Wheatstone bridge. An aftermarket engine control unit (Megasquirt, Model V3.0 mainboard with MS3X expansion) controlled the spark timings, mass of fuel injected, and several other engine parameters, based on inputs like the position of crankshaft and camshaft, amount of intake air, intake air temperature, coolant/oil temperature, and throttle position. Specialized software (TUNERSTUDIO, Version 3.0.28) applied built-in algorithms to determine the correct operating parameters such as spark timing, injection duration, dwell time for spark, etc. A variable reluctance transducer was mounted on a bracket off the crankcase to read 100 equidistant teeth distributed around the flywheel and determine the angular position of the crankshaft. The fuel supply system consisted of a gas cylinder, a pressure regulator, and NG fuel injectors (Rail Spa, Italy, Model IG7 Navajo), shown in Figs. 1(b) and 1(c). A pressure transducer (Kistler, Model 6011) was mounted in the original position of glow plug through a special outer sleeve to collect the in-cylinder pressure trace, shown in Fig. 1(c). A charger amplifier (Kistler, Model 5010) amplified the signal produced by the pressure transducer (0–10 V signal calibrated to bars/volts) and then transmitted it to a DAQ card (National Instruments, Model SCB-68A). An incremental rotary shaft encoder (BEI sensors, Model H25D, resolution 1800) was used to measure engine speed and determine the crankshaft position at any instant. In addition to pressure and speed signals, intake and exhaust temperatures were also collected by DAQ card, which was connected to an I/O device (NI PCIe-6351) on the pressure analysis device to provide usable combustion information such as rate of pressure rise, heat release rate, etc. Outputs from the load cell and LFE's pressure transducers (differential pressure transducer (Ashcroft, Model XLdc) and absolute pressure transducer (GP 50, Model: 211)), and various K-type thermocouples were connected to Ethernet measurement devices (LabJack, Model UE9, and ICP DAS, Model PET7019Z). An in-house built data-acquisition system (DAQ), Scimitar, collected in-cylinder pressure data, air flow rate, coolant and oil temperatures, engine torque, speed, etc., from these two devices. Moreover, the pressure collection and data analysis system used motored pressure to synchronize crankshaft encoder data with engine position. Specifically, peak pressure in the motored pressure trace was applied to determine the difference between the encoder z-pulse and engine top dead center. The procedure was repeated at the beginning, during, and at the end of experiments to ensure that no encoder slippage may affect pressure measurements.

A steady-state parametric study investigated the engine performance and combustion behavior at several operating conditions that changed fuel composition, spark timing (ST), equivalence ratio, and engine speed. The investigated fuels were chemically pure methane (CH_4) and a C_1–C_4 alkane blend (hereafter referred to as NG), with compositions given in Table 2. The parameters in bold italics in Table 3 are for the baseline condition and each test varied one parameter while holding constant for the other two. The operating conditions (low-speed, medium-load, lean-equivalence ratio) were similar to those previously used by the authors for an optical investigation inside the same engine, which

focused on in-cylinder flame propagation [5,6]. The engine was warmed up before testing, and oil and coolant temperatures were maintained constant to eliminate the effects of different boundary conditions on the combustion process. The throttle position in the experiments was fixed to limit the effect of variation of air flow rate on the combustion process.

Results and Discussions

This section describe the operating condition effects on the engine performance based on the in-cylinder pressure trace analysis. As mentioned before, in-cylinder pressure was measured with a piezoelectric pressure transducer, which measures the pressure difference versus time, rather than absolute pressure values. As a result, the pressure signal was "pegged" (i.e., referenced) to the manifold intake pressure. In addition, in-cylinder raw pressure was filtered (see the Appendix for details) to remove the noise caused by a combination of mechanical vibration noise, electric noise, thermal drift, etc. The first 400 individual cycles of each condition were analyzed. The error bars in the Figs. 2, 4, 5, 9, 10, 13 and 14 indicate the 95% confidence interval.

As mentioned in the Introduction section, NG's wider flammability limit allows operation at leaner equivalence ratios. However, lean-burn increases the misfiring probability and the cycle-to-cycle variation, which then influence the engine performance and emissions control. In addition, combustion phasing and duration affect engine performance and emissions through their effects on the in-cylinder heat release. Therefore, the engine performance (such as peak pressure, indicated mean effective pressure (IMEP), η_{th}, etc.), combustion phasing, and cycle-to-cycle variation are presented and discussed next.
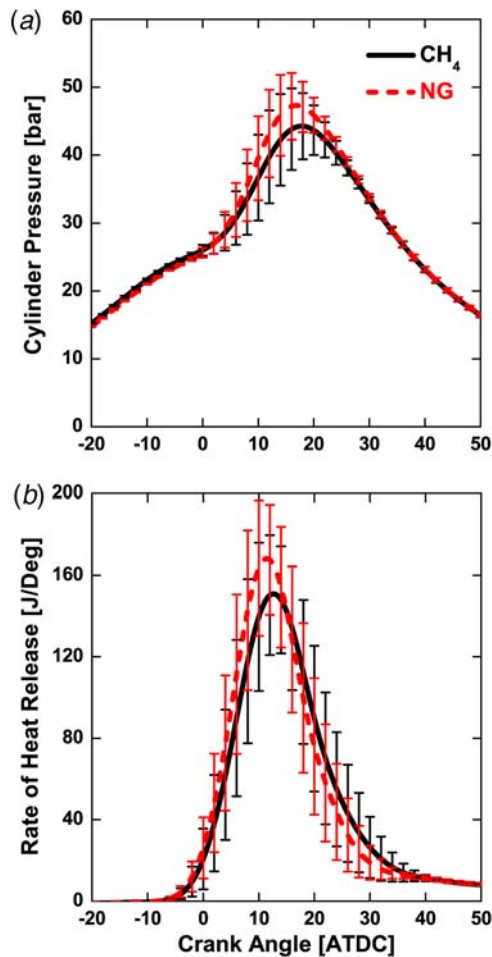
Fig. 2 (*a*) In-cylinder pressure and (*b*) apparent heat release rate, for CH_4 (solid line) and natural gas (dashed line), respectively (baseline conditions)

Fuel Composition Effects. The chemical and thermodynamic properties of non-methane components in the NG may affect the combustion event [34,35]. Consequently, a larger fraction of heavier hydrocarbons or inert components in NG composition is expected to strongly influence engine performance and

combustion characteristics such as ignition ability, aftertreatment durability, fuel economy, engine operability, power output, etc. The in-cylinder pressure trace and rate of heat release of both fuels operated at baseline condition (−10 CA ATDC ST, medium load, and 900 rpm), shown in Fig. 2, are representative of typical homogeneous NG SI combustion. The low slope during the late combusting period was probably due to the shape of the combustion chamber [36]. When the flame front enters the squish region atop the piston crown, the mixture burned slower and more heat was transferred to the boundary. NG had a faster-decreasing slope than CH_4 during the late-combustion period probably due to faster flame propagation and less fuel burned during this period. In addition, the lack of knocking (an important issue for CI engines retrofitted to NG SI operation) proved the choice of spark timing under this low-speed, lean-mixture, and medium-load condition. CA*x* in this study is defined as the crank angle associated with *x*% cumulative heat release, calculated based on Fig. 2. The time in crank angle degrees (CAD) between 5% and 95% heat release is defined as the duration of combustion (DOC). CA50 is defined as the heat release centroid. Table 4 presents the calculated combustion phasing and engine performance comparisons between the two fuels (PP is the peak pressure, LPP is the location of the peak pressure).

Figure 2 and Table 4 show that the peak pressure was higher and advanced for NG compared with CH_4, probably because the presence of higher carbon species enhanced flame speed and the adiabatic flame temperature. In addition, NG increased the power output, evidenced by the 4% higher IMEP, because NG has lower methane number (MN) and higher Wobbe index (WI) compared with CH_4 [37]. In addition, CH_4 had a lower indicated η_{th} compared with NG probably because of (i) NG's higher flame propagation speed which resulted in a more complete combustion, (ii) NG's shorter fast-combustion duration (period before late combusting) overcame the higher heat transfer rate associated with the higher in-cylinder bulk temperature, and (iii) NG's higher low-heating value (LHV) and WI improved the engine performance compared with CH_4 [37]. NG had a higher peak rate of pressure rise (PRRmax) than CH_4, but it was below 2 bars/CA, suggesting that flame propagation was dominant throughout the combustion process. Table 4 also shows that NG has an advanced CA5, CA10, and CA50 compared with CH_4. The time gap between actual spark timing and CA10 is usually defined as the flame development time (ignition delay or lag), and it decreased for NG operation. This phenomenon was possibly due to the presence of higher hydrocarbon chains in the NG. The energy required to break a C–H bond is higher than that to break a C–C bond [38]. As CH_4 does not

Table 4 Performance comparison between CH_4 and NG operation (baseline conditions)

Fuel	PP (bars)	LPP (CA ATDC)	IMEP (bars)	η_{th} (%)	PRR$_{max}$ (bars/CAD)
			Engine performance		
CH_4	44.3	17.8	8.2	36.8	1.6
NG	47.3	16.8	8.5	40.3	2.0

Fuel	CA5 (CA ATDC)	CA10 (CA ATDC)	CA50 (CA ATDC)	CA90 (CA ATDC)	CA95 (CA ATDC)	DOC (CAD)
			Combustion phasing			
CH_4	3.1	5.5	15.0	37.9	54.9	51.8
NG	2.5	4.7	13.5	37.6	54.7	52.2

Fuel	COV$_{IMEP}$ (%)	COV$_{Pmax}$ (%)	STD$_{Pmax}$ (bars)	COV$_{DOC}$ (%)
		Cycle-to-cycle variation		
CH_4	1.06	6.86	3.1	3.36
NG	1.13	5.66	2.7	3.16

contain any C–C bonds, the time required to initiate the combustion process for CH_4 is longer than for other alkanes, which increases its ignition delay [39]. Additionally, CH_4 is less reactive than any other heavier hydrocarbons. Moreover, the addition of lower H/C ratio compounds, like ethane, increased the burning velocity due to the formation of enhanced radicals and more hydrogen particles that accelerated the combustion process [40]. Consequently, the addition of higher hydrocarbons to CH_4 increases the flame speed and generally reduces the overall combustion duration. However, the CA90, CA95, and DOC were similar for NG and CH_4 at the operating conditions investigated here, which can be explained by the diesel-like environment (i.e., part of the mixture burned much more slowly in the squish region, which contributed to much longer late combusting duration). The large cycle-to-cycle variation (caused by lower flame speed and large variations in the unburned fuel mass trapped in the squish region) during the late combusting period, shown in Fig. 2(b), also supports this hypothesis.

Table 4 shows the COV_{IMEP} for both fuels was lower than 2%, indicating stable lean-burn operation. Moreover, the COV_{Pmax} was under 7%, hence the average pressure was considered representative for the condition investigated. To be specific, NG shows the lower coefficient of variation (COV) and the standard deviation of peak pressure, suggesting a lower cycle-to-cycle variation compared with CH_4. This can be explained by the addition of heavier hydrocarbons to CH_4, which improved the ignition process and increased the flame propagation speed, in turn helping to decrease the cycle-to-cycle variation [41]. In addition to the peak pressure variation, Fig. 2(b) also shows less variation of the apparent heat release rate (AHRR) for NG during the late combusting period. Considering the small percentage of higher hydrocarbons for NG shown in Table 3, it seems that even small amounts of higher species of hydrocarbon additives produced a more stable combustion process compared with CH_4 only.

Spark Timing Effects. Spark timing (ST) affects combustion efficiency and stability through its effect on spark inception and flame propagation [19]. This study swept the ST from −30 CA ATDC to −10 CA ATDC at constant engine speed (900 rpm) and load ($\phi = 0.73$, medium load). Figures 3–5 present the ST effects on engine performance and combustion characteristics of NG SI operation in a reentrant bowl combustion chamber. As expected, advanced ST increased and advanced the location of maximum pressure and increased the rate of pressure rise (PRR). However, the peak PRR was always below 4 bars/CA, indicating flame propagation dominated during the combustion event.

In addition, the error bars indicate that some cycles with advanced ST had similar combustion as cycles at delayed ST, evidenced by the overlapping of peak pressure and its location in Fig. 4. As variations in the spark intensity and location together with the variation in local turbulence and mixture equivalence ratio at the spark plug location affect the early flame development, the overlapping was probably due to these variations. Heat release analysis describes the efficiency of converting the thermal energy of the fuel into work done by the engine. For a constant supply of chemical energy, a higher heat release indicates that more work is done by the system, which means the engine is more efficient. Figure 3(b) shows that the heat release rate of CH_4 at a −20 CA ATDC ST was larger than at another ST. As expected, Fig. 4(b) shows that −20 CA ATDC ST was the maximum brake torque (MBT) ST for the load and equivalence ratio investigated here, supported by the higher IMEP and η_{th}. Advancing the ST from this optimum will advance and increase cylinder pressure before TDC, which would oppose the piston's upward movement. Then, more work will be done during the compression stroke against the piston movement compared with optimum ST, which would reduce the amount of power delivered to the crankshaft. Although retarding the ST can result in peak cylinder pressure to occur later in the expansion stroke, this will lower peak pressure hence decrease the work done on the piston.
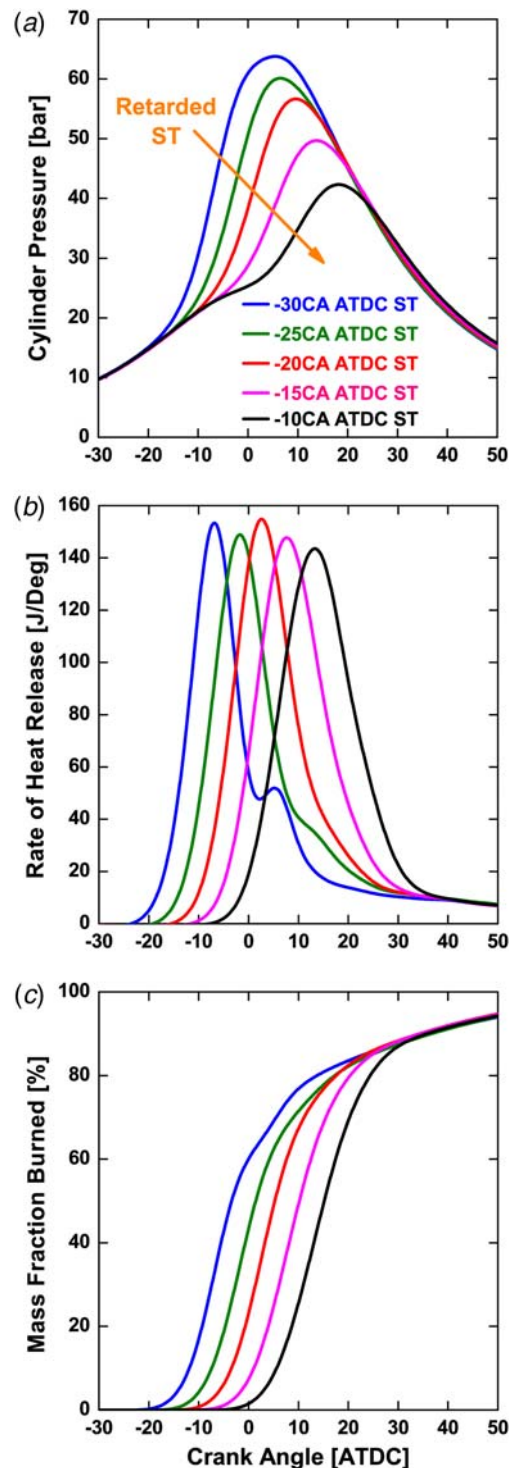

Fig. 3 Effect of spark timing on (a) in-cylinder pressure, (b) apparent heat release rate, and (c) mass fraction burned, for CH_4

The heat release analysis also shows a second peak on the heat release rate for −30 CA ATDC ST. Moreover, −25 CA ATDC ST shows significant late burn, suggesting that an important fuel fraction was burned late in the cycle, also evidenced by the corresponding MFB shown in Fig. 3(c). Four hundred consecutive cycles were plotted in Fig. 6 to investigate late-combustion differences compared to the average data shown in Fig. 3(b). Figure 6 shows several cycles with significant late combustion even for −10 CA ATDC ST, which indicated that the averaged data can hide important characteristics of NG SI
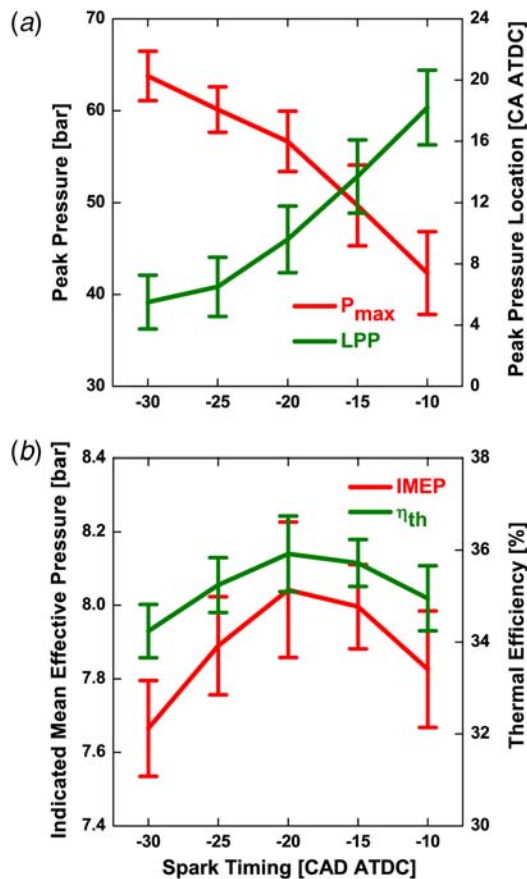
Fig. 4 Effect of spark timing on (*a*) peak pressure and its location and (*b*) IMEP and thermal efficiency
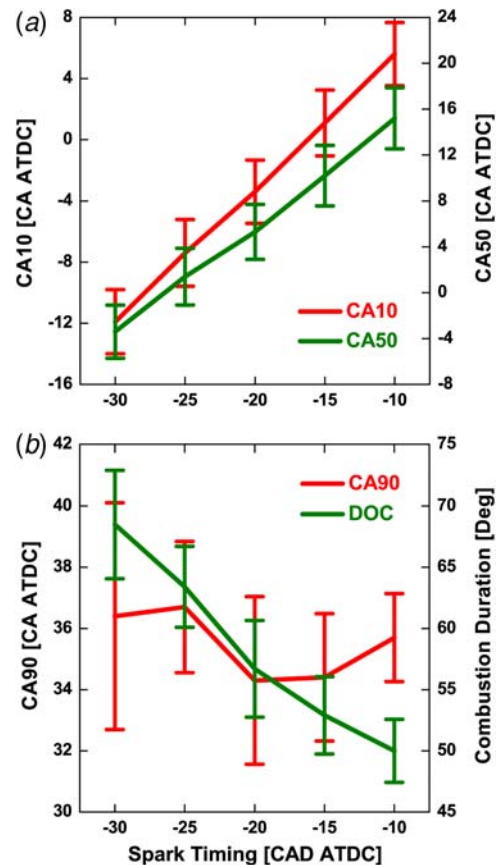

Fig. 5 Effect of spark timing on (*a*) CA10 and CA50 and (*b*) CA90 and combustion duration

combustion in a bowl-in-piston chamber. Moreover, -15 CA ATDC ST suggests more frequent and higher-intensity burn during the late-combustion period. The late burn was more visible at -20 CA ATDC ST, and the double heat release peak started to be visible frequently at -25 CA ATDC ST. Finally, almost all the cycles at -30 CA ATDC ST show the second peak heat release rate, but with different phasing and intensity. Overall, late burn phenomenon was seen at all conditions irrespective of the ST. This two-zone combustion phenomenon was probably due to the typical bowl-in-piston chamber that trapped an important mass fraction of the mixture in the squish volume, which then burned in the late-combustion period. When the squish height was small, the burning speed decreased in this region, probably due to the high surface-to-volume ratio, lower local turbulence, increased heat transfer to the boundary, and decreased the temperature of the unburned mixture in front of the flame. As the squish height increased during the power stroke, the surface-to-volume ratio decreased, which increased the burning speed and the rate of which the fuel was consumed, hence the late burn seen at advanced ST and at several individual cycles with delayed ST. However, there was no obvious late burn phenomenon for delayed ST, probably because the phasing of the inside- and outside-the-bowl combustion was very close. For advanced ST, the phasing of these two combusting events was more separated and, as a result, the significant late burn was visible.

Figure 3(*c*), which shows the mass fraction burned for CH_4 at various STs, suggests an almost similar end of combustion (EOC) for the five cases despite the 20 CA difference in ST. Figure 5 presents the combusting phasing calculated based on mass fraction burned. Both CA10 and CA50 were retarded with retarded ST. Moreover, the differences in the actual CA10 and CA50 values

between cases were similar to their difference in ST, which suggest a similar flame development and flame speed before CA50. However, the CA90 was nearly the same, which implies that the DOC decreased with spark timing retardation, probably due to the different late burn mentioned earlier.
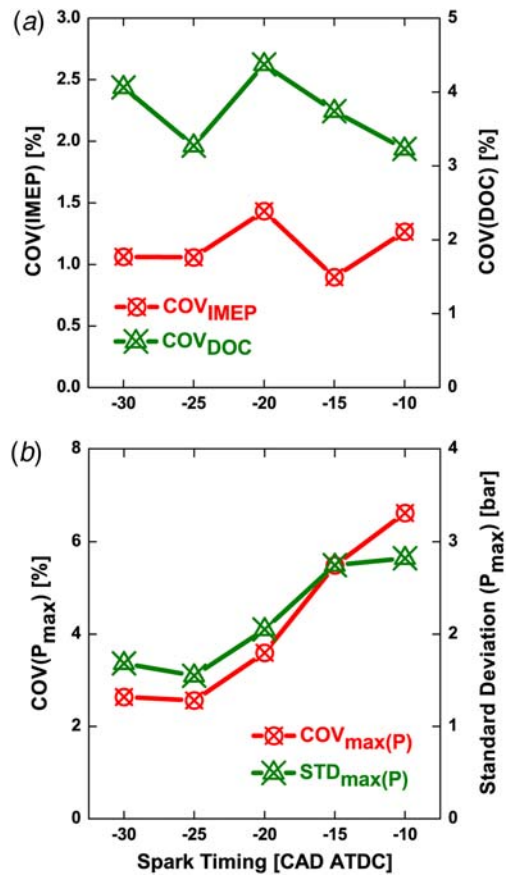
The COV of IMEP (COV_{IMEP}) is a common estimator of cycle-to-cycle variation. COV_{IMEP} should be smaller than 5% for stable engine operation. Other methods to evaluate the cycle-to-cycle variation include COV and standard deviation (STD) of peak pressure (i.e., COV_{Pmax} and STD_{Pmax}), and COV of combustion duration (COV_{DOC}) [36]. IMEP measures engine's capacity to do work and is independent of engine displacement. IMEP can be considered as the mean pressure acting on a piston during compression and expansion strokes. In other words, IMEP is a parameter that characterizes the whole combustion event. Consequently, the COV of IMEP is a coefficient related to the whole combustion event [36]. Similarly, COV of DOC can be regarded as a qualitative cycle-integrated parameter [36]. In contrast, peak pressure was affected by the history of spark inception and the subsequent fully developed turbulent flame propagation, but not affected by the late combusting period. Therefore, COV and STD of peak pressure only partial characterize the combustion event.

The lack of knocking and small COV_{IMEP} and COV_{DOC} values (shown in Fig. 7(*a*)) suggest stable combustion at all investigated STs. Advanced ST decreases the cycle-to-cycle variation because it shifts the flame propagation at more favorable in-cylinder conditions for flame development. The same was true for COV_{Pmax} and STD_{Pmax} except at -30 CA ATDC ST (as shown in Fig. 7(*b*)), which can be explained by the late-combustion effects. In detail, Fig. 3 indicates that, for the average pressure trace, the maximum pressure location was close to the position of the second peak of heat release rate located (also evidenced by reduced peak-growth
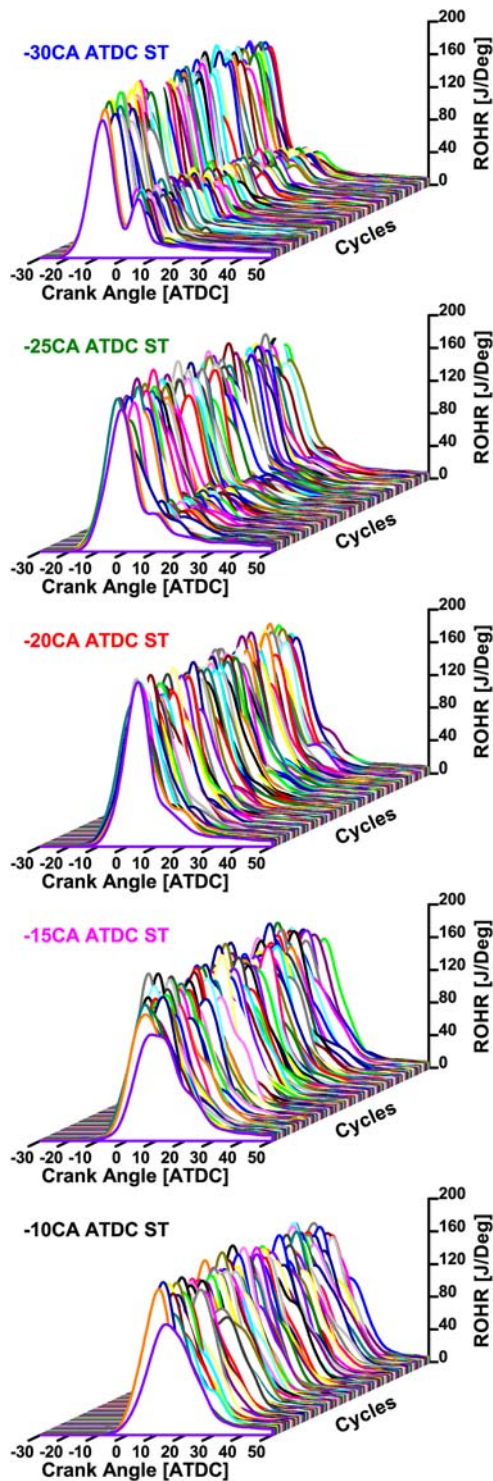
Fig. 6 Effect of spark timing on the apparent heat release rate of individual engine cycles

Fig. 7 Effect of spark timing on (a) COV_{IMEP} and COV_{DOC} and (b) COV_{Pmax} and STD_{Pmax}

trend at −30 CA ATDC ST compared with delayed ST), which is also true for individual cycles. It can be concluded that the different phasing/intensity of the second heat release peak (shown in Fig. 6) during the late burning period largely increased the variations in the peak cylinder pressure for −30 CA ATDC ST. As to COV_{IMEP} and COV_{DOC}, they did not show the expected trend (i.e., advanced ST decreases the cycle-to-cycle variation, similar to the trend of COV_{Pmax} and STD_{Pmax}), which indicates that the generally used estimator, COV_{IMEP}, was not enough to evaluate the cycle-to-cycle variation for NG SI burning in diesel-like environment under the

conditions investigated here. This was also probably due to the COV_{IMEP} being affected by the late-combustion event, in addition to many other factors such as the spark intensity/location, turbulence around spark and in the main combustion chamber, fuel composition, piston geometry, operating conditions (spark timing, load, speed, and mixture equivalence ratio), etc.

Equivalence Ratio Effects. Equivalence ratio (ϕ) is a fundamental engine operating variable. This work investigated the effect of ϕ at medium-load conditions, using a constant engine speed (900 rpm), spark timing (−10 CA ATDC ST), and intake temperature and pressure. While ST was not optimized for changed equivalence ratio conditions, the comparisons shown in Figs. 8–10 show the influence of ϕ on the performance and combustion characteristics for NG SI lean combustion. Figures 8(a) and 9(a) show that a higher ϕ increased the cylinder pressure and advanced and increased peak pressure. NG maximum pressure rise rate increased with ϕ but was below 2.5 bars/CA. Figure 8(b) indicates that the heat release rate increased with ϕ due to the increase in available chemical energy every cycle. Moreover, the decrease in the AHRR magnitude during the late combusting period was larger at higher ϕ, probably due to a faster heat release during the main combusting period (i.e., from TDC to 15 CA ATDC), which reduced the percentage of fuel burning in late-combustion stages. Under lean conditions, a higher amount of fuel accelerated the flame development and propagation, resulting in higher power output (i.e., IMEP) from the engine, as seen in Fig. 9(b). In addition, η_{th} of NG was higher than that of CH_4, which suggests that NG was better at the operating conditions investigated in this work.

Higher ϕ at a constant speed usually increases the burning speed which leads to a more complete combustion process. However, the amount of unburned fuel trapped in the crevices would also increase with ϕ. This trade-off can explain the peak efficiencies shown in
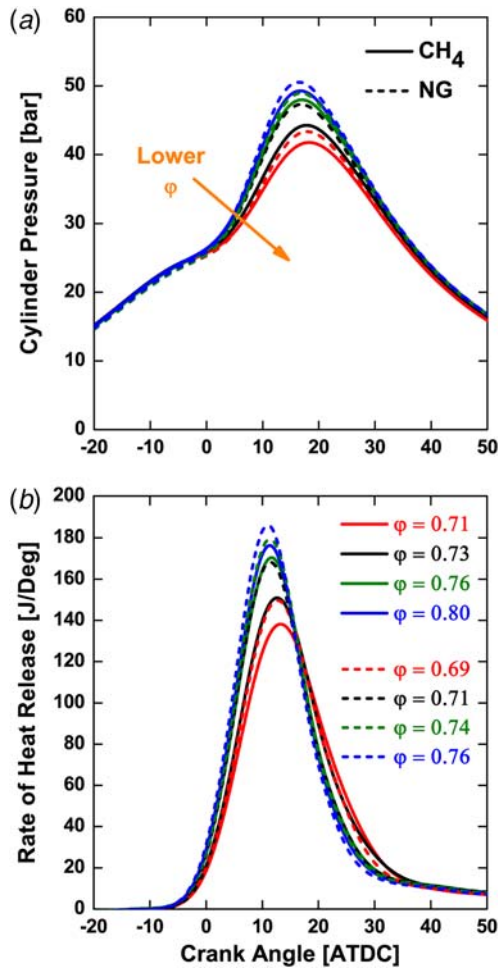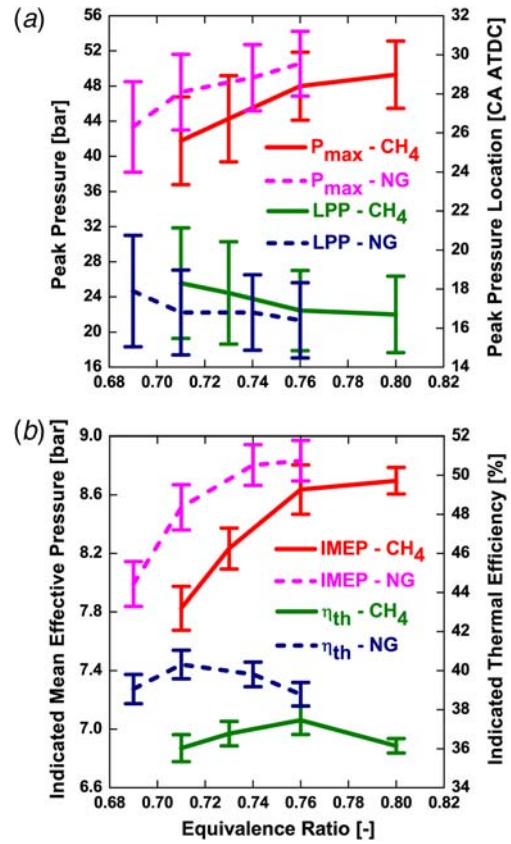
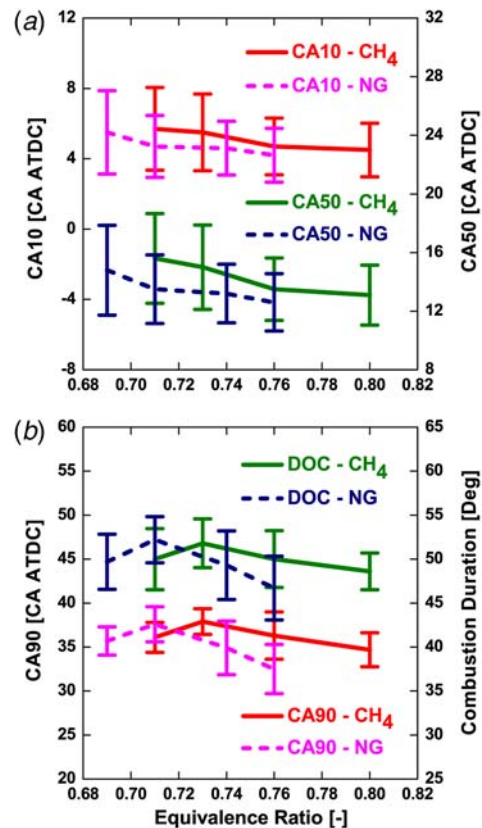Fig. 8 Effect of equivalence ratio on (a) in-cylinder pressure and (b) apparent heat release rate

Fig. 9 Effect of equivalence ratio on (a) peak pressure and its locations and (b) IMEP and thermal efficiency

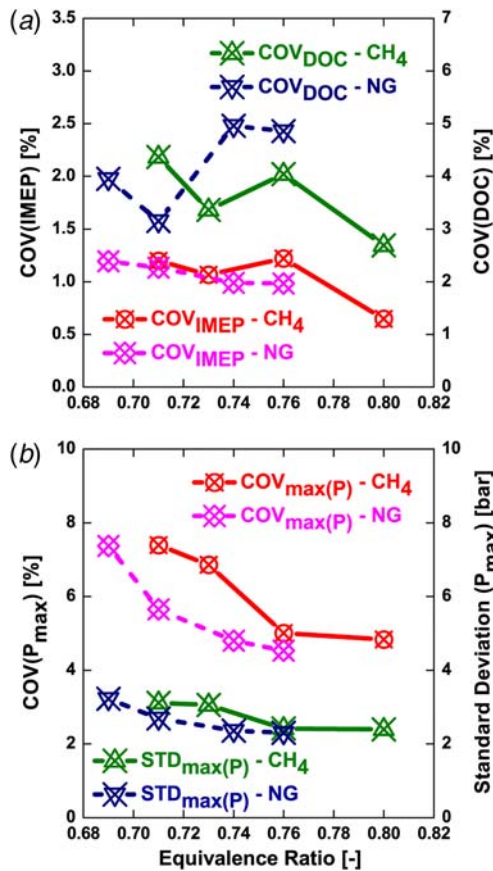Fig. 10 Effect of equivalence ratio on (a) CA10 and CA50 and (b) CA90 and combustion duration (DOC)

Fig. 9(b). Moreover, NG had the peak η_{th} at a lower ϕ, suggesting that NG may run leaner than CH_4 at similar efficiency.

Figure 10 shows CA10 and CA50 advanced with higher ϕ, which can be explained by the addition of hydrocarbons with higher flame speed compared to CH_4. However, there was no correlation for the DOC or CA90, probably due to the two-zone combustion. As ϕ decreases, the air to fuel ratio increases, resulting in a lower adiabatic flame speed and occasional flame quenching and/or misfiring, especially when compared with stoichiometric operation [19]. The relatively small values for COV_{IMEP} and COV_{DOC} shown in Fig. 11(a) help alleviate this concern. Generally, a faster flame propagation can compensate for the differences in flame inception, hence decreasing the cycle-to-cycle variation. This can be achieved by increasing the equivalence ratio or using a faster-burning fuel. The COV_{Pmax} and STD_{Pmax}, shown in Fig. 11(b), agree well with this logic. However, the COV_{IMEP} and COV_{DOC} shown in Fig. 11(a) were not correlated with ϕ, probably due to the late burn effects, which suggests that more parameters (such as COV_{Pmax} and STD_{Pmax}) are needed to correlate the cycle-to-cycle variations.

Engine Speed Effects. Generally, engine speed affects in-cylinder gas motion, friction, trapped mass, volumetric efficiency, flame propagation speed, the time available to complete combustion, and the heat transfer rates [19]. At higher engine speed, the heat release rates are predominately affected by the frictional losses of the engine. Although the higher turbulence generated by increased engine speed would accelerate flame propagation, the overall combustion process will be also affected

Fig. 11 Effect of equivalence ratio on (a) COV_{IMEP} and COV_{DOC} and (b) COV_{Pmax} and STD_{Pmax}

Fig. 12 Effect of engine speed on (a) in-cylinder pressure and (b) apparent heat release rate

by the reduced residence time (mainly for the period between ST and exhaust valve opening), hence a higher probability of incomplete combustion. Therefore, it is preferred to maintain a mid-range engine speed, where high pressures can compensate the frictional losses and provide better operating conditions. Moreover, the ST must be advanced with increased engine speed to provide more time for completing the combustion event. In this study, the engine speed was increased from 900 rpm to 1300 rpm in 100 rpm increments, at constant ST (−10 CA ATDC) and ϕ (medium load), hence the combustion phasing was not optimized at higher speeds considering the relatively small range of engine sweep. Higher speed decreased PRR (below 2 bars/CA). Therefore, there was no evidence of detonation/knock and flame propagation dominated the combustion event.

Figure 12(a) shows that in-cylinder pressure decreased with engine speed due to lower volumetric efficiency (see the decrease in pressure at the beginning of the compression stroke for the higher-speed conditions) and the non-optimized ST. NG had higher peak pressure values than CH_4 probably due to the higher energy content compared with CH_4 (see the differences in WI in Table 2). Figures 12(a) and 13(a) show that increased engine speed decreased and delayed the maximum pressure for both CH_4 and NG, probably due to less time available to complete combustion at constant ST settings. Also, NG has always advanced peak pressure location compared with CH_4, suggesting that the addition of ethane and propane in the NG composition increased the flame speed irrespective of the engine speed. The large overlapping of 95% confidence interval shown in Fig. 13 indicates similar individual cycles despite the different fuel composition and operating conditions. Figure 12(b) shows that the highest heat release was at 900 rpm, which also had the maximum efficiency for this speed sweep. A lower peak pressure and heat release rate in Fig. 12(b) suggest that less work per cycle, which affected the engine power
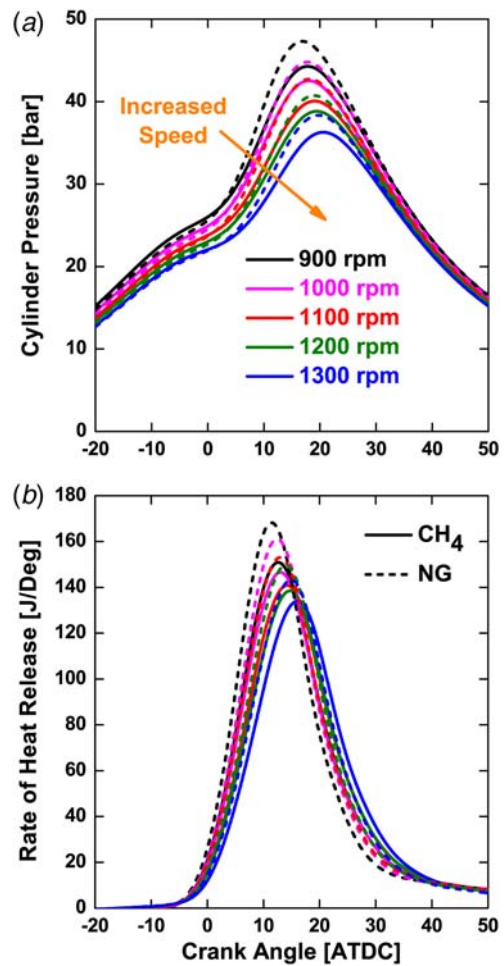
output. Hence, the IMEP and η_{th} decreased linearly with the increase in speed, as shown in Fig. 13(b). The hypothesis of a better combustion process for NG was supported by the higher IMEP and η_{th} than CH_4.

Figure 14(a) shows that a higher engine speed retarded CA10 and CA50. The addition of ethane and propane improved flame inception, which can explain the advanced CA10 for NG. Moreover, the difference in CA50 between fuels was larger than that of CA10, suggesting that NG had also a faster flame development probably due to the larger laminar flame speed of NG and, which can also be inferred from the larger increase in the heat release rate magnitude during fast combusting period, as shown in Fig. 12(b). However, Fig. 14(b) shows that engine speed had negligible effects on the CA90 and combustion duration. It suggests that mixture burning inside the squish region was dominated by changes in the local environment with the engine speed.

Figure 15(a) shows a low COV_{IMEP} irrespective of engine speed and fuel, suggesting no misfire cycles existed even under higher speed. As ethane and propane have better ignition quality and faster laminar flame speed compared with CH_4, the cycle-to-cycle variation of NG should be lower than CH_4, which was supported by the COV_{Pmax} and STD_{Pmax} shown in Fig. 15(b). It is also interesting that the STD_{Pmax} decreased with engine speed, probably due to the less time available for fuel to burn and the faster flame speed that decreased the differences in peak pressure under the premise of a good spark-ignition event and no misfiring. However, COV_{IMEP} and COV_{DOC} shown in Fig. 15(a) did not show any correlation with speed. This suggests that COV_{Pmax} and STD_{Pmax} would be

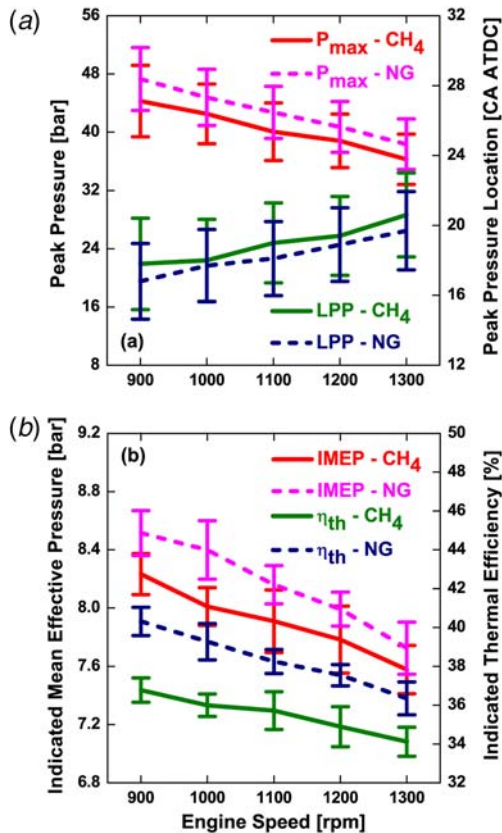**Fig. 13** Effect of engine speed on (*a*) peak pressure and its location and (*b*) IMEP and thermal efficiency
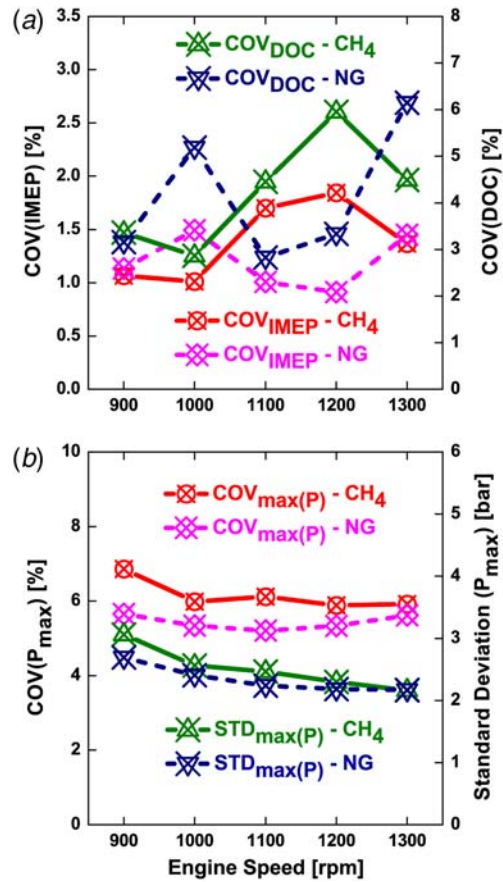

Fig. 14 Effect of engine speed on (*a*) CA10 and CA50 and (*b*) CA90 and combustion duration

Fig. 15 Effect of engine speed on (*a*) COV_{IMEP} and COV_{DOC} and (*b*) COV_{Pmax} and STD_{Pmax}

better to evaluate the cycle-to-cycle variation for two-zone combustion, while COV_{IMEP} and COV_{DOC} that recorded the whole history of combustion would be good to evaluate power output variations that may affect vehicle drivability.

Summary and Conclusions

Converting heavy-duty diesel engines to NG SI operation by adding a spark plug to ignite the fuel and fumigating NG inside the intake manifold is a simple and efficient use of NG in the transportation sector. Better knowledge of NG combustion inside geometries representative of heavy-duty CI engines can accelerate their conversion to NG operation. As a result, this study describes an experimental investigation that changed NG composition, spark timing, equivalence ratio, and engine speed. The experiments were performed in a single-cylinder heavy-duty CI engine modified to NG SI operation, by replacing the fuel injector with an NG spark plug and adding port fuel injection to air inlet for fuel delivery. The major conclusions of this study were

- The NG SI combustion inside a bowl-in-piston combustion chamber can result in a two-zone event, with a significant late burn or even double-peak heat release. This was probably due to an important fuel fraction experiencing slow and late burning inside the squish region Advanced spark timing showed more frequent and higher intensity of this late burn phenomenon.
- Peak pressure and its location, IMEP, η_{th}, CA10, and CA50 were correlated to changes in the fuel composition, spark timing, equivalence ratio, and engine speed. Specifically, NG had always a better power output and faster flame propagation regardless of the operating conditions, probably due to the addition of heavier hydrocarbons that increased the WI, ignition

quality, and flame propagation speed. Delayed spark timing, lower ϕ, and higher engine speed would decrease the peak pressure, IMEP, and retard the CA10, CA50, and LPP. However, CA90 and combustion duration did not show any strong relations, probably due to the late combustion that was mainly controlled by the local phenomena inside the squish region such as the local turbulence intensity, gas motion direction, height of squish region, mass of trapped fuel, and heat transfer to the boundary. In addition, COV_{Pmax} and STD_{Pmax} are better for evaluating the cycle-to-cycle variation for the combustion event investigated here compared with the COV_{IMEP} and COV_{DOC} because they were less affected by the late burn phenomenon.

- The low COV_{IMEP} and moderate rate of pressure rise for all the conditions investigated here suggested that flame propagation dominated and a stable combustion event. The lack of knocking in this 13.3 compression ratio engine showed promise for conventional heavy-duty CI engines converted to NG SI operation under medium load and low-speed conditions.

Acknowledgment

Funding Data

Nomenclature

AHRR = apparent heat release rate
ATDC = after top dead center
BTDC = before top dead center
CAD = crank angle degree
CAx = CAD corresponding to x% mass fraction burned
COV = coefficient of variation
DOC = combustion duration
EOC = end of combustion
IMEP = indicated mean effective pressure
LHV = lower heating value
LPP = peak pressure location
MBT = maximum brake torque
MFB = mass fraction burned
MN = methane number
MON = motor octane number
PRR = rate of pressure rise
SOC = start of combustion
ST = spark timing
STD = standard deviation
TDC = top dead center
WI = Wobbe index
ϕ = equivalence ratio
η_{th} = thermal efficiency

Appendix: In-Cylinder Pressure Filtering

Non-flush mounting of the pressure transducer created standing/resonant waves in the access passage, which affected the recorded pressure fidelity by introducing undesired noise. The noise in this work was removed by applying a Savitzky-Golay FIR smoothing
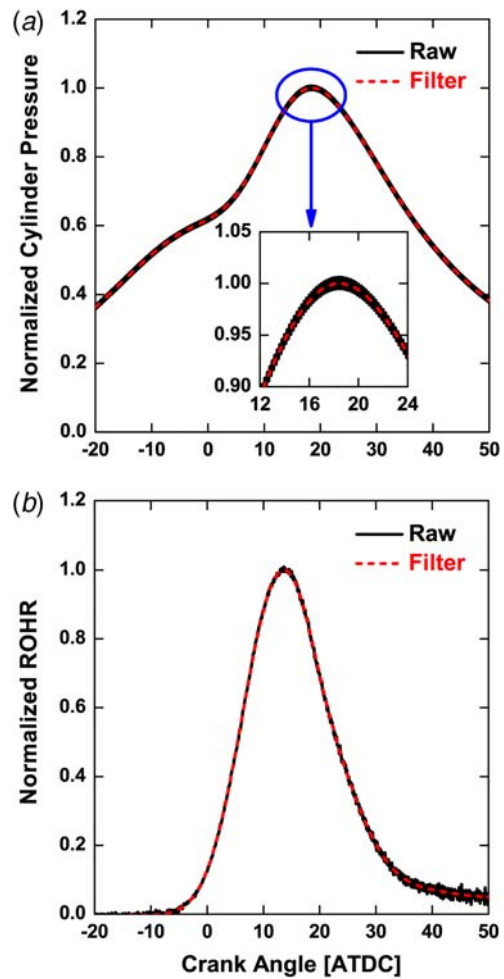
Fig. 16 (*a*) Raw and filtered in-cylinder pressure trace and (*b*) rate of heat release calculated from raw and filtered pressure trace

filter to the recorded pressure trace. The procedure was done using the sgolayfilt (*x*, order, framelem) function in a MATLAB® environment. Figure 16 shows an example of raw (unfiltered) and filtered pressure trace, and the corresponding apparent heat release rate derived from it.

References

[1] Gupta, M., Bell, S., and Tillman, S., 1996, "An Investigation of Lean Combustion in a Natural Gas-Fueled Spark-Ignited Engine," ASME J. Energy Resour. Technol., **118**(2), pp. 145–151.
[2] Xu, H., and LaPointe, L. A., 2015, "Combustion Characteristics of Lean Burn and Stoichiometric With Exhaust Gas Recirculation Spark-Ignited Natural Gas Engines," ASME J. Eng. Gas Turbines Power, **137**(11), p. 111511.
[3] Weaver, C. S., 1989, "Natural Gas Vehicles—A Review of the State of the Art," SAE Technical Paper 892133.
[4] Beck, N. J., 1990, "Natural Gas—A Rational Approach to Clean Air," SAE Technical Paper 902228.
[5] Dumitrescu, C. E., Padmanaban, V., and Liu, J., 2018, "An Experimental Investigation of Early Flame Development in an Optical SI Engine Fueled With Natural Gas," ASME J. Eng. Gas Turbines Power, **140**(8), p. 082802.
[6] Liu, J., and Dumitrescu, C. E., 2018, "Combustion Visualization in a Single-Cylinder Heavy-Duty CI Engine Converted to Natural Gas SI Operation," Proceedings of the Eastern States Section of the Combustion Institute's Spring Technical Meeting, State College, PA, Mar. 4–7, Paper 3C06.
[7] Jones, M. G. K., and Heaton, D. M., 1989, "Nebula Combustion System for Lean Burn Spark Ignited Gas Engines," SAE Technical Paper 890211.
[8] Bommisetty, H., Liu, J., Kooragayala, R., and Dumitrescu, C., 2018, "Fuel Composition Effects in a CI Engine Converted to SI Natural Gas Operation," SAE Technical Paper 2018-01-1137.
[9] Germane, G. J., Wood, C. G., and Hess, C. C., 1983, "Lean Combustion in Spark-Ignited Internal Combustion Engines—A Review," SAE Technical Paper 831694.

[10] Bolt, J. A., and Holkeboer, D. H., 1962, "Lean Fuel/Air Mixtures for High-Compression Spark-Ignited Engines," SAE Technical Paper 620524.

[11] Cartellieri, W., Chmela, F., Kapus, P., and Tatschl, R., 1994, "Mechanisms Leading to Stable and Efficient Combustion in Lean Burn Gas Engines," Proceedings of the International Symposium COMODIA, Yokohama, Japan, July 11–14, Paper C94P017.

[12] McTaggart-Cowan, G. P., Reynolds, C. C. O., and Bushe, W. K., 2006, "Natural Gas Fuelling for Heavy-Duty On-Road Use: Current Trends and Future Direction," Int. J. Environ. Stud., 63(4), pp. 421–440.

[13] Liu, J., and Dumitrescu, C. E., 2018, "3D CFD Simulation of a CI Engine Converted to SI Natural Gas Operation Using the G-Equation," Fuel, 232(1), pp. 833–844.

[14] Donateo, T., Tornese, F., and Laforgia, D., 2013, "Computer-Aided Conversion of an Engine From Diesel to Methane," Appl. Energy, 108(1), pp. 8–23.

[15] Zheng, J., Chen, X., Hu, T., and Zhan, Z., 2013, "The Research Development in Direct Injection Spark-Ignition Natural Gas Engine," Proceedings of the FISITA 2012 World Automotive Congress, Beijing, China, Nov. 27–30, pp. 51–63.

[16] Zheng, J., Huang, Z., Wang, J., Wang, B., Ning, D., and Zhang, Y., 2009, "Effect of Compression Ratio on Cycle-by-Cycle Variations in a Natural Gas Direct Injection Engine," Energy Fuels, 23(11), pp. 5357–5366.

[17] Polcyn, N., Lai, M.-C., and Lee, P.-I., 2014, "Investigation of Ignition Energy With Visualization on a Spark Ignited Engine Powered by CNG," SAE Technical Paper 2014-01-1331.

[18] Karim, G. A., and Wierzba, I., 1989, "Experimental and Analytical Studies of the Lean Operational Limits in Methane Fueled Spark Ignition and Compression Ignition Engines," SAE Technical Paper 891637.

[19] Heywood, J. B., 1988, Internal Combustion Engine Fundamentals, McGraw-Hill, New York.

[20] Unich, A., Bata, R. M., and Lyons, D. W., 1993, "Natural Gas: A Promising Fuel for I.C. Engines," SAE Technical Paper 930929.

[21] Meyer, R., Meyers, D., Shahed, S. M., and Duggal, V. K., 1992, "Development of a Heavy Duty On-Highway Natural Gas-Fueled Engine," SAE Technical Paper 922362.

[22] Johansson, B., and Olsson, K., 1995, "Combustion Chambers for Natural Gas SI Engines Part 1: Fluid Flow and Combustion," SAE Technical Paper 950469.

[23] Olsson, K., and Johansson, B., 1995, "Combustion Chambers for Natural Gas SI Engines Part 2: Combustion and Emissions," SAE Technical Paper 950517.

[24] Van Der Weide, J., Seppen, J. J., Van Ling, J. A. N., and Dekker, H. J., 1988, "Experiences With CNG and LPG Operated Heavy Duty Vehicles With Emphasis on US HD Diesel Emission Standards," SAE Technical Paper 881657.

[25] Shiells, W., and Garcia, P., 1988, "Experience With the Operation of Heavy Vehicle Engines Dedicated to the Use of CNG and LPG Fuels," First International Conference and Exhibition on Natural Gas Vehicles, Sydney, Australia, Oct. 27–30.

[26] Raine, R. R., Stephenson, J., and Elder, S. T., 1988, "Characteristics of Diesel Engines Converted to Spark Ignition Operation Fuelled With Natural Gas," SAE Technical Paper 880149.

[27] Goto, S., Lee, D., Harayama, N., Honjo, F., Ueno, H., Honma, H., Wakao, Y., and Mori, M., 2000, "Development of LPG SI and CI Engine for Heavy Duty Vehicles," Proceedings of the Seoul 2000 FISITA World Automotive Congress, Seoul, June 12, pp. 394–403.

[28] Goto, S., Lee, D., Shakal, J., Harayama, N., Honjyo, F., and Ueno, H., 1999, "Performance and Emissions of an LPG Lean-Burn Engine for Heavy Duty Vehicles," SAE Technical Paper 1999-01-1513.

[29] Lee, D., Goto, S., Kim, I., and Motohashi, M., 1999, "Spectroscopic Investigation of the Combustion Process in an LPG Lean-Burn SI Engine," SAE Technical Paper 1999-01-3510.

[30] Lee, D., Shakal, J., Goto, S., Ishikawa, H., Ueno, H., and Harayama, N., 1999, "Observation of Flame Propagation in an LPG Lean Burn SI Engine," SAE Technical Paper 1999-01-0570.

[31] Donateo, T., de Risi, A., and Laforgia, D., 2012, "On the Computer-Aided Conversion of a Diesel Engine to CNG-Dedicated or Dual Fuel Combustion Regime," Proceedings of the ASME 2012 Internal Combustion Engine Division Spring Technical Conference, Torino, Piemonte, Italy, May 6–9, No. ICES2012-81090, pp. 933–943.

[32] Jiao, Y., Zhang, H., Yang, Z., Zhang, Z., and Si, P., 2008, "Multi-Dimensional Simulation of Combustion Process in Ignition Nature Gas Engine," J. Therm. Sci. Technol., 7(4), pp. 360–366.

[33] Yin, Y., Liu, S., and Tian, Y., 2010, "Numerical Simulation for the Combustion Process of Spark Ignition CNG Engine," Intern. Combust. Engine Powerplant, 3(1), pp. 008.

[34] Langness, C., and Depcik, C., 2016, "Statistical Analyses of CNG Constituents on Dual-Fuel Compression Ignition Combustion," SAE Technical Paper 2016-01-0802.

[35] Langness, C., Mattson, J., and Depcik, C., 2017, "Moderate Substitution of Varying Compressed Natural Gas Constituents for Assisted Diesel Combustion," Combust. Sci. Technol., 189(8), pp. 1354–1372.

[36] Reyes, M., Tinaut, F. V., Gimenez, B., and Perez, A., 2014, "Characterization of Cycle-to-Cycle Variations in a Natural Gas Spark Ignition Engine," Fuel, 140(1), pp. 752–761.

[37] Kim, K., Kim, H., Kim, B., and Lee, K., 2009, "Effect of Natural Gas Composition on the Performance of a CNG Engine," Oil Gas Sci. Technol.—Rev. IFP, 64(2), pp. 199–206.

[38] Burcat, A., Scheller, K., and Lifshitz, A., 1971, "Shock-Tube Investigation of Comparative Ignition Delay Times for C1-C5 Alkanes," Combust. Flame, 16(1), pp. 29–33.

[39] Spadaccini, L. J., and Colket, M. B., 1994, "Ignition Delay Characteristics of Methane Fuels," Prog. Energy Combust. Sci., 20(5), pp. 431–460.

[40] McTaggart-Cowan, G. P., Rogak, S. N., Munshi, S. R., Hill, P. G., and Bushe, W. K., 2010, "The Influence of Fuel Composition on a Heavy-Duty, Natural-Gas Direct-Injection Engine," Fuel, 89(3), pp. 752–759.

[41] Kreutzer, C. J., Olsen, D. B., and Bremmer, R. J., 2011, "Evaluation of a Lean-Burn Natural Gas Engine Operating on Variable Methane Number Fuel," Proceedings of the ASME 2011 Internal Combustion Engine Division Fall Technical Conference, Morgantown, WV, Oct. 2–5, No. ICEF2011-60071, pp. 159–166.